

# A Novel Encoded Particle Technology that Enables Simultaneous Interrogation of Multiple Cell Types

OREN BESKE, JINJIAO GUO, JIANREN LI, DANIEL BASSONI, KIMBERLY BLAND, HOLLY MARCINIAK, MIKE ZAROWITZ, VLADIMIR TEMOV, ILYA RAVKIN, and SIMON GOLDBARD

The authors have developed a cellular analysis platform, based on encoded microcarriers, that enables the multiplexed analysis of a diverse range of cellular assays. At the core of this technology are classes of microcarriers that have unique, identifiable codes that are deciphered using CCD-based imaging and subsequent image analysis. The platform is compatible with a wide variety of cellular imaging-based assays, including calcium flux, reporter gene activation, cytotoxicity, and proliferation. In addition, the platform is compatible with both colorimetric and fluorescent readouts. Notably, this technology has the unique ability to multiplex different cell lines in a single microplate well, enabling scientists to perform assays and data analysis in novel ways. (*Journal of Biomolecular Screening* 2004:173-185)

**Key words:** multiplexing, imaging, cell-based assays, particle technology, cells, microarrays

## INTRODUCTION

**T**HE COLLECTION OF LARGE DATA SETS via parallel processing is now firmly embedded in biological and drug discovery research due to the implementation of microarrays.<sup>1-6</sup> The implementation of such multiplexing technologies is recognized to have clear advantages: decreased reagent usage, smaller sample requirement, speed, and the robustness of using internal controls for comparisons. In the prototypic DNA array format, the identity of each element is determined by its position within the array. As an alternative to positional arrays, new technologies are beginning to emerge that generate nonpositional arrays.<sup>6-8</sup>

As the name implies, nonpositional arrays do not rely on the position of an element within the array to determine its identity. Rather, each element is identified by its association with a unique code. The exact natures of these codes range from colors to radio frequencies.<sup>9-11</sup> Regardless of the encoding technique, these technologies result in an array that is more flexible and amenable to a

broader range of applications than the aforementioned positional approach. Although both positional and nonpositional approaches can be applied widely to the analysis of nucleic acids and proteins, there are only a few examples in which they have been applied to the analysis of cells.<sup>8,12</sup>

In this article, we present an approach that demonstrates the feasibility of generating nonpositional arrays that can be used in the analysis of cells. This platform employs encoded carriers (ECs) to which different reagents can be attached or on which cells can be grown. The encoding strategy, which does not interfere with data collection, invokes the use of differently colored bands alternated at unique positions. The particles are imaged using a CCD-based system and subsequently decoded via software. Image analysis algorithms extract the assay data and associate them with the proper code. The ECs demonstrate no inherent cellular toxicity and are compatible with multiple readout modalities. Here we present proof-of-principle examples of how the technology can be applied to the study of receptor pharmacology and the screening of potential antitumor compounds.

## RESULTS AND DISCUSSION

*Encoded particle approach to multiplexing assays.* The encoded microcarriers (ECs) that we have developed are shown in Figure 1A. The encoding strategy consists of an expandable barcode comprising 4 colored bands (Fig. 1A, small arrow), 2 on

Vitro Bioscience, Inc., Mountain View, CA.

Received Jun 3, 2003, and in revised form Sep 16, 2003. Accepted for publication Sep 18, 2003.

*Journal of Biomolecular Screening* 9(3); 2004  
DOI: 10.1177/1087057103260088

Published by Sage Publications in association with The Society for Biomolecular Screening

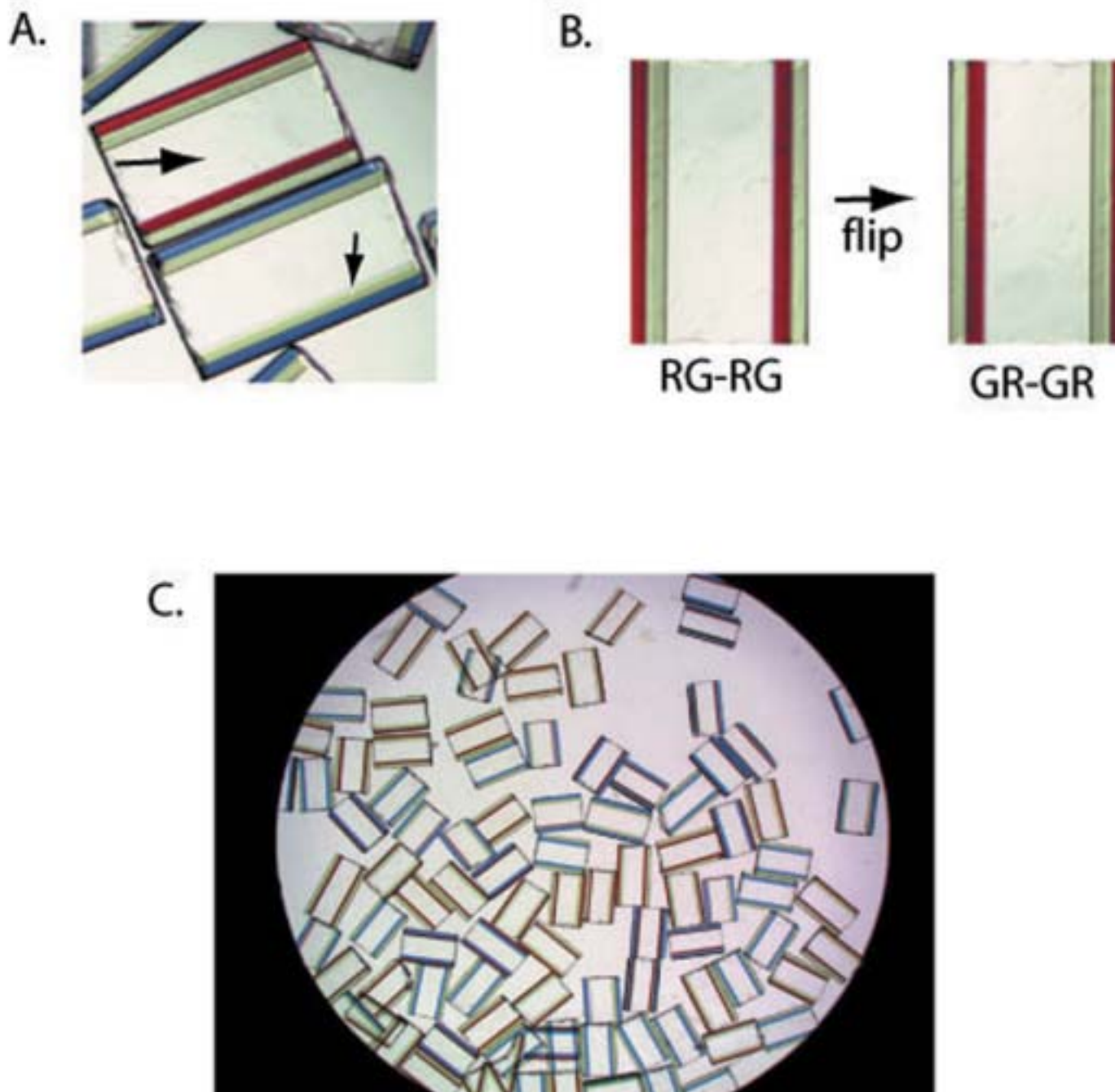


**FIG. 1.** Encoded particle approach. (A) The encoding particles are shown. These particles are roughly  $350 \times 550 \mu\text{m}$  and are  $90 \mu\text{m}$  thick. There are 2 sets of colored coding bands (small arrow) on either side of an optically clear section (big arrow). The code is determined by the combination of colors at each of the 4 positions. (B) This figure demonstrates why all theoretical code possibilities cannot be used. In this case, the code Red/Green–Red/Green can be read Green/Red–Green/Red if it is flipped over. (C) This image shows the dispersion of the encoded particles within a single well of a 96-well microplate. In this well, there are approximately 90 particles.

each side of an optically clear data readout section (Fig. 1A, large arrow). A distinguishing characteristic of the particles is that the area from which the assay data are gathered is physically separated from the code bands. Therefore, there is no physical overlap of the

coding information with the data and hence no cross-talk or limitation of one imposed on the other. That is, the encoding strategy does not limit the number of fluorophores that can be used to gather data. This encoding strategy is expandable in that the num-

ber of unique codes manufactured can be scaled by altering the number of colored bands, the number of colors used in the bands, or both.

Theoretically, the total possible codes (T) is the number of bands (B) raised to the power of the number of colors used (C);  $T = C^B$ . However, because the ECs land randomly on a surface, either side up, some of the code possibilities must be eliminated as nonunique. For example, if the code Red-Green-Clear-Red-Green (RG-RG) lands on its other side, it will read Green-Red-Clear-Green-Red (GR-GR, Fig. 1B). Therefore, only one of these potential codes can be used at a time. In addition, to aid software recognition of the code, another constraint is imposed. A color is not allowed to appear directly next to itself on the same side of the clear section. With these limitations taken into consideration, the encoding power as it relates to the number of colors used is shown in Table 1. For the initial implementation of the technology and the multiplexing of cell-based assays, we have chosen an approach with 3 colors and therefore a potential multiplex factor of 21.

The ECs are rectangular and flat and can be manufactured from multiple materials. Because the decoding strategy and the cellular assays require CCD-based imaging technologies, the ECs must be in the same focal plane. Therefore, the particles are manufactured such that their aspect ratio and density ensure that they lay flat on the bottom surface when placed in aqueous media, for example, at the bottom of a microplate well. In addition, surface features have been engineered into the ECs to protect the cells from physical stress during their handling.

The current size of the particles ( $350 \times 550 \times 90 \mu\text{m}$ ) has been optimized for cellular assays in a 96-well format. When an experiment is performed, the ECs with unique codes and associated cells are mixed and dispensed into the microplate well (Fig. 2). The dispensing step results in the generation of an array of carriers randomly dispersed throughout the well. We have adopted an imaging strategy such that the entire well can be viewed in a single image. One such image of a microplate well containing approximately 90 dispensed ECs is shown in Figure 1C. In contrast to traditional positional arrays, each particle contains a code, and therefore random dispersion of the ECs has no effect on the decoding of the array. The array is decoded via an image analysis algorithm that identifies the carriers and their codes. In addition, the algorithm determines if the carrier should be used for further data analysis. For example, some particles may overlap, resulting in unreadable codes or superimposed data readout sections. In such cases, the software algorithms eliminate that particle from subsequent analysis. To ensure that no data are lost, multiple instances (i.e., 5-10) of each code are present in each well. Therefore, given that a microplate well (96-well format) can accommodate 90 ECs in each well, the practical multiplexing limit is 18 codes per well.

*Multiplexing a cell-based receptor-signaling assay: Calcium flux.* To demonstrate feasibility of adapting a calcium flux assay to encoded carriers, a Chinese hamster ovary-derived cell line that stably expresses the human bradykinin-2 receptor (CHO-hB2) was seeded onto ECs and dispensed into a microplate well. After

**Table 1.** Relationship between the Number of Coding Bands, Numbers of Colors Used, and Number of Allowed Codes

Number of Coding Bands	Number of Colors	Total Number of Allowed Codes
4	2	3
4	3	21
4	4	78

loading the cells with the calcium-sensitive dye Fluo-4, a preligand addition image was taken (Fig. 3A, -Ligand). A faint fluorescence is seen in these cells that represents a combination of the dye-loading efficiency and the endogenous calcium levels in unstimulated cells. Kallidin, a bradykinin receptor agonist,<sup>13</sup> was then added and another image acquired. As expected, the CHO-hB2 cells show a significant increase in fluorescence after the addition of kallidin (Fig. 3A, +Ligand). This demonstrates that the ECs did not affect the ability of these cells to respond to ligand and that robust fluorescent cellular images can be acquired with our imaging approach.

Having shown that we can image a calcium-flux assay on the ECs, we then multiplexed this assay using 3 cell lines: the previously described CHO-hB2 cell line, HEK-293, and CHO. The HEK-293 cells endogenously express the muscarinic acetylcholine receptors (mAChR). The CHO cell line is the parental line to the CHO-hB2 cells and expresses neither the mAChR nor the hB2R. These cell lines were individually plated onto ECs with unique codes. After an overnight incubation, the ECs with attached cells were then mixed and dispensed into a 96-well plate. After loading the cells with Fluo-4, images were acquired and quantified by the methods described in the experimental protocol section. The ligand conditions included either kallidin (hB2 agonist) alone, carbachol (AChR agonist) alone, or both. When either kallidin or carbachol was added, selective activation of CHO-hB2 and 293 cells, respectively, was observed (data not shown). When both ligands were added together, both CHO-hB2 and 293 cells exhibited a rapid rise in fluorescent intensity followed by a slow, gradual decrease (Fig. 3B). As expected, the CHO cells, which do not express receptors that can be agonized by these ligands, showed no significant increase in fluorescent signal and therefore serve as an internal control. These data provide evidence that it is possible to multiplex calcium-flux assays using our ECs and collect kinetic data from multiple cell lines within a single microplate well. In addition, this demonstrates that having multiple cell lines present in a single well did not alter their ability to respond selectively to these ligands.

*Multiplexing a cell-based receptor-signaling assay: Reporter gene.* A  $\beta$ -galactosidase reporter gene system was used to test the feasibility of implementing reporter gene assays on ECs. The system chosen was one used to assay Gs-coupled G-protein-coupled receptors (GPCRs), the activation of which results in an increase in

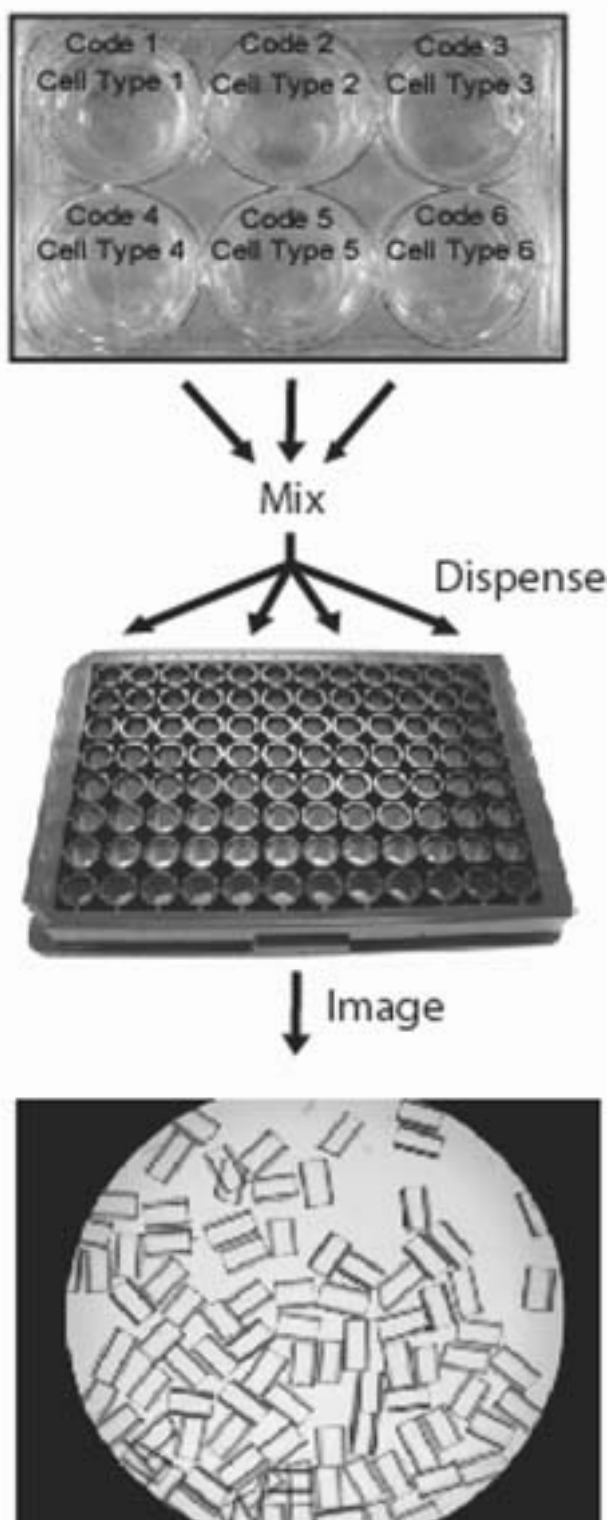


**FIG. 2.** This scheme represents the outline of how cell-based assays are performed using our encoded carrier technology. First, each cell type is grown on a carrier with a unique code. The cells/carriers are then mixed together and dispensed into a 96-well microplate. The assay protocol is then carried out in the microplate and the data gathered by imaging.

cAMP response element-binding protein (CREB)-dependent transcription via the CREB response element (CRE).<sup>14,15</sup> Therefore, we used a plasmid containing the  $\beta$ -gal gene downstream of multiple CREs. Activation of the Gs signaling pathway in cells transfected with the CRE  $\beta$ -gal reporter plasmid results in  $\beta$ -gal expression.<sup>16</sup> Visualization of reporter gene activity was via a colorimetric staining protocol using an X-gal reagent that stains  $\beta$ -gal-expressing cells with a blue intracellular precipitate (Fig. 4A, +Ligand).

To test the feasibility of applying this approach to encoded carriers, HEK-293 cells were transiently cotransfected with a DH receptor expression vector and the CRE  $\beta$ -gal reporter plasmid. The cells were then plated onto ECs, mixed, and subsequently dispensed into a 96-well plate. They were then incubated in the presence or absence of diuretic hormone for 5 h, fixed, stained, and imaged. This assay is colorimetric, and hence no fluorescent images were acquired. The acquisition of bright-field images serves to both decode the particles as well as gather the biological data. Images from representative wells with and without ligand are shown in Figure 4A. The cells in the presence of DH show a distinct increase in blue staining, demonstrating that the DH receptor was functionally activated, resulting in detectable  $\beta$ -gal expression.

Having demonstrated the feasibility of assaying Gs-coupled GPCRs using this system on ECs, we then multiplexed the assay across 8 different cell types. Each of these cell types were HEK-293s transiently transfected with different sets of plasmids. The experiment consisted of 5 Gs-coupled GPCRs—pituitary adenylate cyclase activating peptide-1 (PAC1) receptor, vasoactive intestinal peptide-1 (VIP1) receptor, vasoactive intestinal peptide-2 (VIP2) receptor, melanocortin-3 (MC3) receptor, and the diuretic hormone (DH) receptor—cotransfected with the CRE  $\beta$ -gal reporter plasmid. In addition, we transfected HEK-293s with a nuclear hormone receptor, the ecdysone (Ecd) receptor. This was included to demonstrate that different signaling pathways could be analyzed simultaneously. Two control cell types were also included. The positive control cells (POS) were transfected with a plasmid that contains a cytomegalovirus (CMV) promoter driving  $\beta$ -gal expression. These cells express  $\beta$ -galactosidase constitutively and therefore serve as a control for staining, imaging, and image analysis. In addition, in the case of an inhibition assay, this control would ensure that any inhibitory activity identified was acting at the level of receptor signaling rather than inhibiting reporter gene,  $\beta$ -gal, activity. The other control cell type (NEG) was transfected with the CRE  $\beta$ -gal reporter alone. This control serves to ensure that any agonist activity identified was dependent on the heterologous expression of the GPCR in question and not acting on the reporter plasmid directly (i.e., through activation of an endogenously expressed receptor).

These 8 cell types—5 Gs GPCRs, 1 nuclear hormone receptor, and 2 controls—were plated onto carriers with different codes. These carriers and attached cells were mixed and dispensed into a plate. Then, either no compound or known agonists were added individually to separate wells. The cells were subsequently incu-

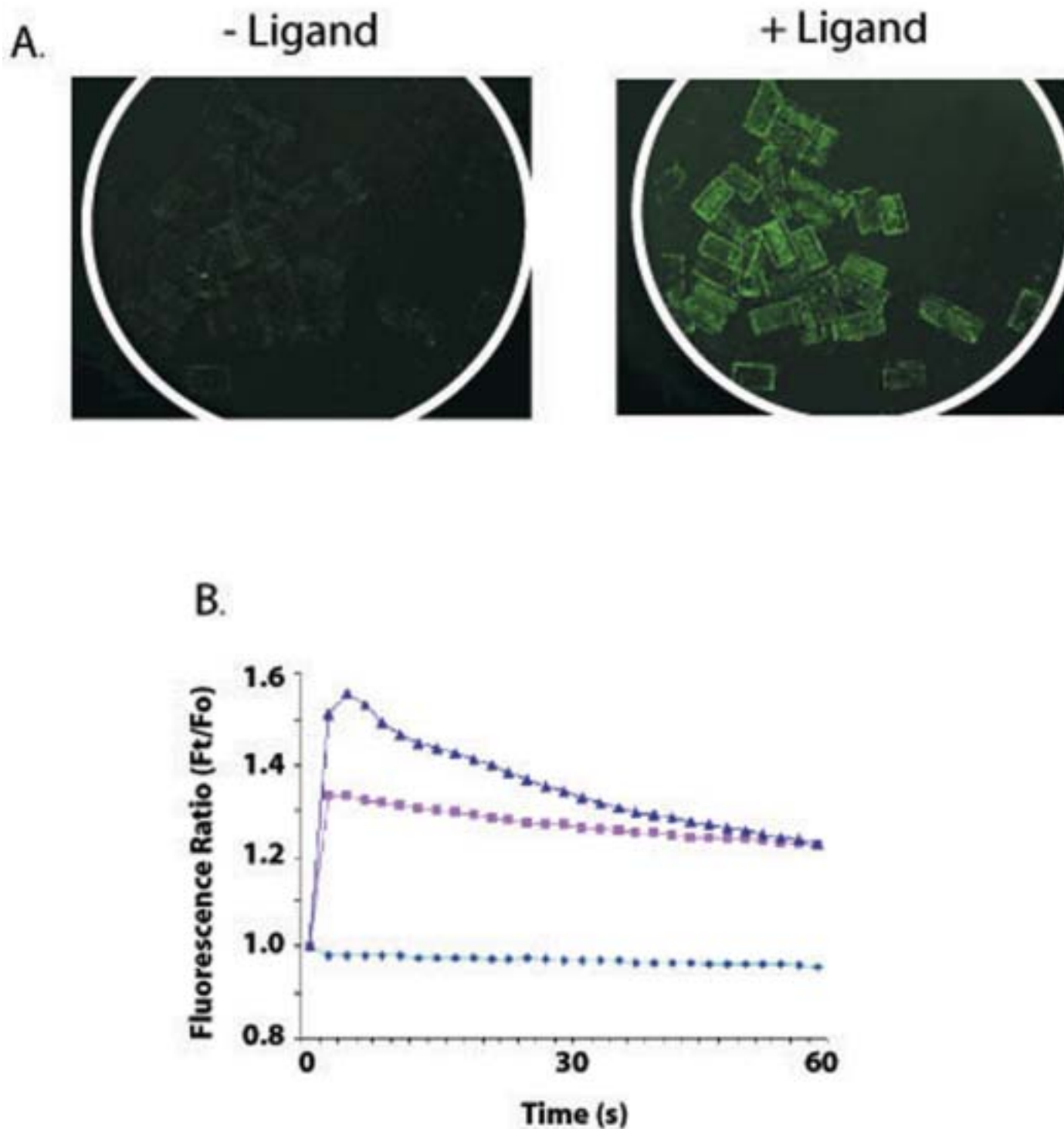


**FIG. 3.** Application of the technology to calcium signaling. (A) CHO-hB2 cells grown on encoded carriers were loaded with the calcium-sensitive dye Fluo-4 and subsequently treated with the bradykinin receptor agonist kallidin. The left image was taken before ligand addition, and the right image was acquired after ligand addition. (B) Graph of a kinetic calcium-flux experiment multiplexed across 3 cell types; well CHO-hB2 (pink trace), CHO (teal trace), and 293 cells (blue trace). An image was taken before compound addition, and then the compound was added manually and images acquired every 2 sec for 1 min. The fluorescent intensity at each time point was divided by the intensity before compound addition and graphed versus time. Both kallidin (1  $\mu$ M) and carbachol (100  $\mu$ M) were added, which agonize the bradykinin and the acetylcholine receptors expressed in the CHO-hB2 cells and 293 cells, respectively. CHO cells do not endogenously express either of these 2 receptors, and therefore no calcium signal was detected.

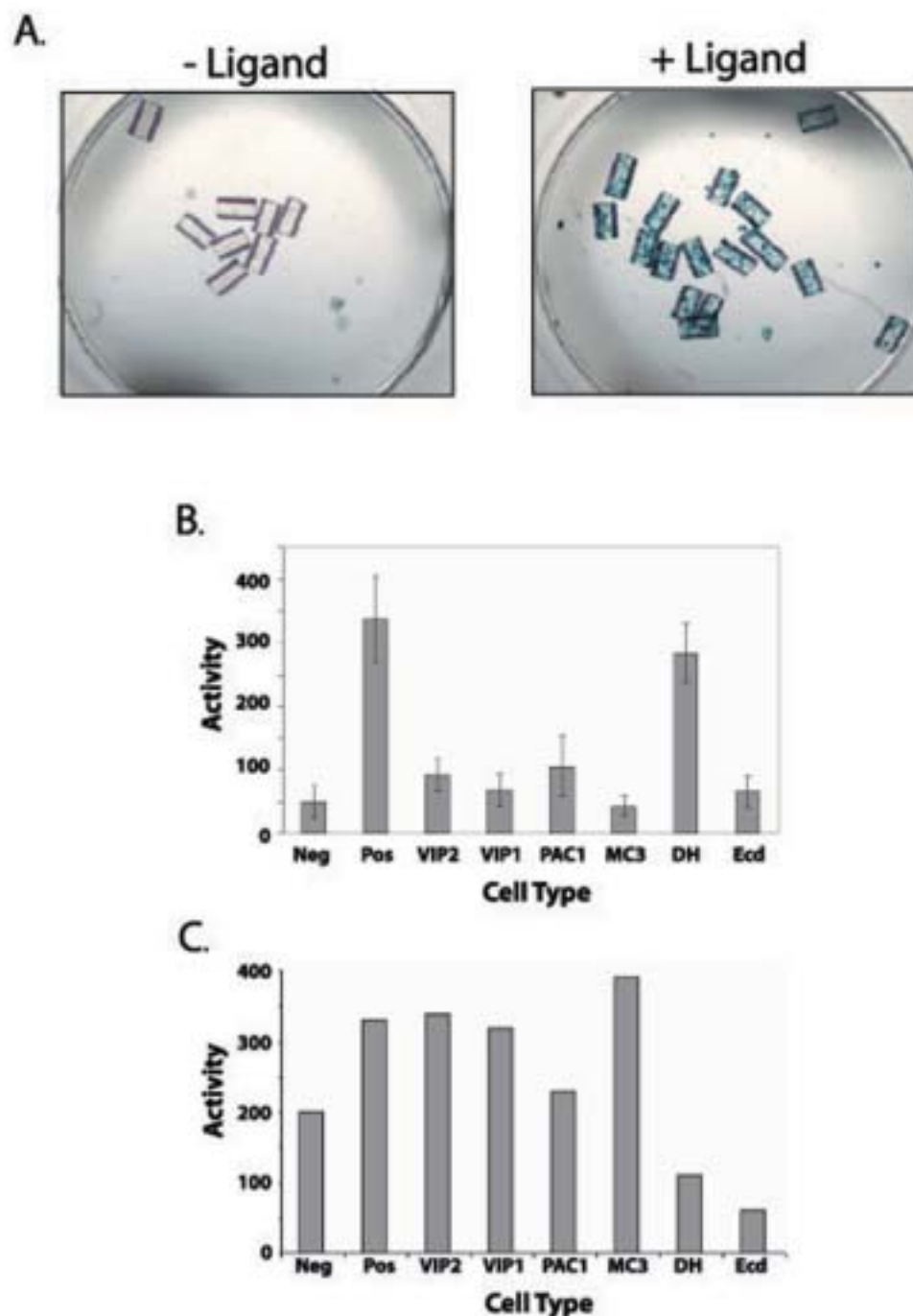


**FIG. 4.** Multiplexing of a  $\beta$ -gal reporter gene assay. (A) HEK-293 cells were transiently cotransfected with the diuretic hormone receptor and the CREB response element (CRE)  $\beta$ -gal reporter plasmid and subsequently plated onto carriers and dispensed into a 96-well plate. The images show the signal generated by X-gal staining of  $\beta$ -gal activity in the absence (left image) and presence (right image) of 100  $\mu$ M diuretic hormone. (B) Data from a multiplex experiment that included 8 transiently transfected cell types: 6 experimental and 2 controls. Five of the cell types (VIP2, VIP1, PAC1, MC3, and DH) were transiently transfected with Gs-coupled G-protein-coupled receptors (GPCRs) and the pCRE  $\beta$ -gal reporter plasmid. The Ecd cell type represents 293 cells stably expressing the ecdysone receptor and transiently transfected with the pIND/ $\beta$ -gal reporter plasmid. The positive (POS) and negative (NEG) control cells were transfected with pCMV  $\beta$ -gal and pCRE  $\beta$ -gal, respectively. Each cell type was grown on carriers of different codes, mixed together, and assayed. The data shown here are the average and standard deviation of triplicate wells to which 100  $\mu$ M diuretic hormone was added. (C) Data from a single well of a multiplexed experiment that included the same cell types as in B. The cells were assayed for activity across multiple ligands, and the result from a single well is shown. The compound displays a nonselective activation of multiple GPCRs expressing cells as well as the negative control. The Ecd cell line, designed to read out a different pathway than the GPCRs, showed no response to this ligand, suggesting that the activation observed was specific to the GPCR signaling pathway.

bated, stained, imaged, and quantified. The quantification algorithm used to analyze these images calculated a relative activity that takes into account both the number of stained cells and the intensity of staining. The raw data, averages, and standard deviations, from 3 replicate wells treated with 100  $\mu$ M diuretic hormone, are shown in Figure 4B. The controls behave as expected, showing low and high  $\beta$ -gal activity values for the NEG and POS cells, respectively. Furthermore, all of the receptors show baseline activity except the diuretic hormone receptor, which shows a 5- to 6-fold increase in activity over the negative control. This is also expected because it is known that the diuretic hormone is a selective agonist for the DH receptor. We were able to show selective agonism for all the receptors in this experiment when the cognate ligand was added to the well (data not shown). Importantly, these data also demonstrate that having these cell lines sharing a common extracellular environment did not affect their abilities to respond to selective ligands.

We assayed the response of this set of cell lines across a number of known pharmacologically active compounds. We identified a nonselective agonist, and the data from that well are shown in Figure 4C. It stimulated  $\beta$ -gal expression in many of the GPCR-transfected cell lines (cf. Fig. 4B,C) as well as the negative control cell line (cf. NEG in Fig. 4B,C). The activation of the reporter plasmid-only transfected cell line (NEG) suggests that much of the activity observed in the GPCR-transfected cells is independent of the heterologously expressed GPCR and is the result of an activity on the reporter plasmid alone (i.e., via activation of an endogenous receptor). The Ecd cells show a background level of activation. This suggests that the nonselective activity identified is acting on the GPCR pathway and not the Ecd pathway. These data demonstrate the feasibility of using EC technology to simultaneously profile a compound's activity across multiple receptors.

In addition, the choice of cell types allowed the assay to be performed using internal assay controls and pathway controls. Therefore, this type of experimental design not only resulted in the collection of both potency and selectivity data but also mechanistic information from a single well. Figure 4C demonstrates that the compound identified acts nonselectively across the GPCRs, and its mechanism is via the Gs-GPCR pathway rather than the ecdysone pathway. Multiplexing cellular assays enables this type of analysis and will be very powerful in identifying the signaling pathways of orphan receptors as well as elucidating the mechanisms of action of potential therapeutics.

*Multiplexing a cell-based cytotoxicity assay.* Profiling compounds by virtue of their cytotoxic and antiproliferative effects is often used to profile potential anticancer agents.<sup>17,18</sup> In addition, the cell-type selectivity of such agents is routinely assessed. This type of analysis is well suited for a cell-based multiplexing technology because activity and selectivity can be assessed within a single well. Therefore, we tested to see if these assay protocols were compatible with EC-based multiplexing.

A compromise in plasma membrane integrity is a phenotype of cells exposed to cytotoxic agents.<sup>19</sup> Using a reagent that stains cells with intact membranes green and those with compromised membranes red, we tested the compatibility of this protocol with ECs. To this end, cells were grown on 2 carrier codes: 1 was untreated, and the other code was treated with methanol to fix and permeabilize the cells. These were then mixed, dispensed, stained, and imaged. A representative image of these wells is shown in Figure 5A. The cells that were untreated, and therefore have intact membranes, stained green (Fig. 5A, small arrow), whereas the methanol-treated cells were red (Fig. 5A, large arrow). This demonstrated the feasibility of applying the encoded carrier platform to this cytotoxicity assay. Therefore, we proceeded with a multiplexed dose curve experiment.

Nine cell lines (Hela, CHO, CV1, COS7, A549, 3T3, HCT116, OVCAR3, MCF7) representing different tissue and organismal origins were grown on ECs with 9 unique codes. After mixing and dispensing the ECs and attached cells, they were incubated with increasing amounts of DMSO for 24 h. The cells were stained and imaged. The images from a representative dose curve are shown in Figure 5B. At 1% DMSO, nearly all of the cells are stained green, indicating that the plasma membranes are not affected by this concentration. As the DMSO concentration rises to 10% and 20%, there is a concomitant increase in the amount of red staining. At 40% DMSO, only red staining is evident, showing that all of the cellular membranes have been compromised at this concentration. Quantification of the data as a percentage of dead cells (red staining) to all cells (both red and green staining) resulted in a measure of the amount of killing at each dose.

The dose curve for A549 cells derived from the above images (Fig. 5B) is shown in Figure 5C. The quantification of the images shows a dose-dependent effect on how many of the cells stained red, culminating at 100% with the 40% DMSO treatment. Similar curves were generated for the other 8 cell lines that were in each of these wells (data not shown). These experiments demonstrate that this encoded particle technology enables the use of this cytotoxicity assay to generate dose curves for multiple cell lines simultaneously.

*Proliferation.* Proliferation assays are commonly used in the identification and evaluation of novel and existing antitumor agents. An image-based 5-Bromo-deoxyuracil (BrdU) incorporation assay was developed to measure the transition of cells through the S-phase, a correlate of proliferative index.<sup>20,21</sup> In this protocol, living cells are incubated with BrdU, which is used as a substrate by cellular DNA polymerases, resulting in the nucleotide analog being incorporated into newly synthesized DNA.<sup>21</sup> The incorporated BrdU is then detected with a fluorescently labeled anti-BrdU antibody. To aid in the quantification of the images, all nuclei were stained with the DNA binding dye 7-amino-actinomycin D (7AAD). To test if cells grown on ECs were compatible with this staining technique, MCF7 cells were grown on encoded carriers,

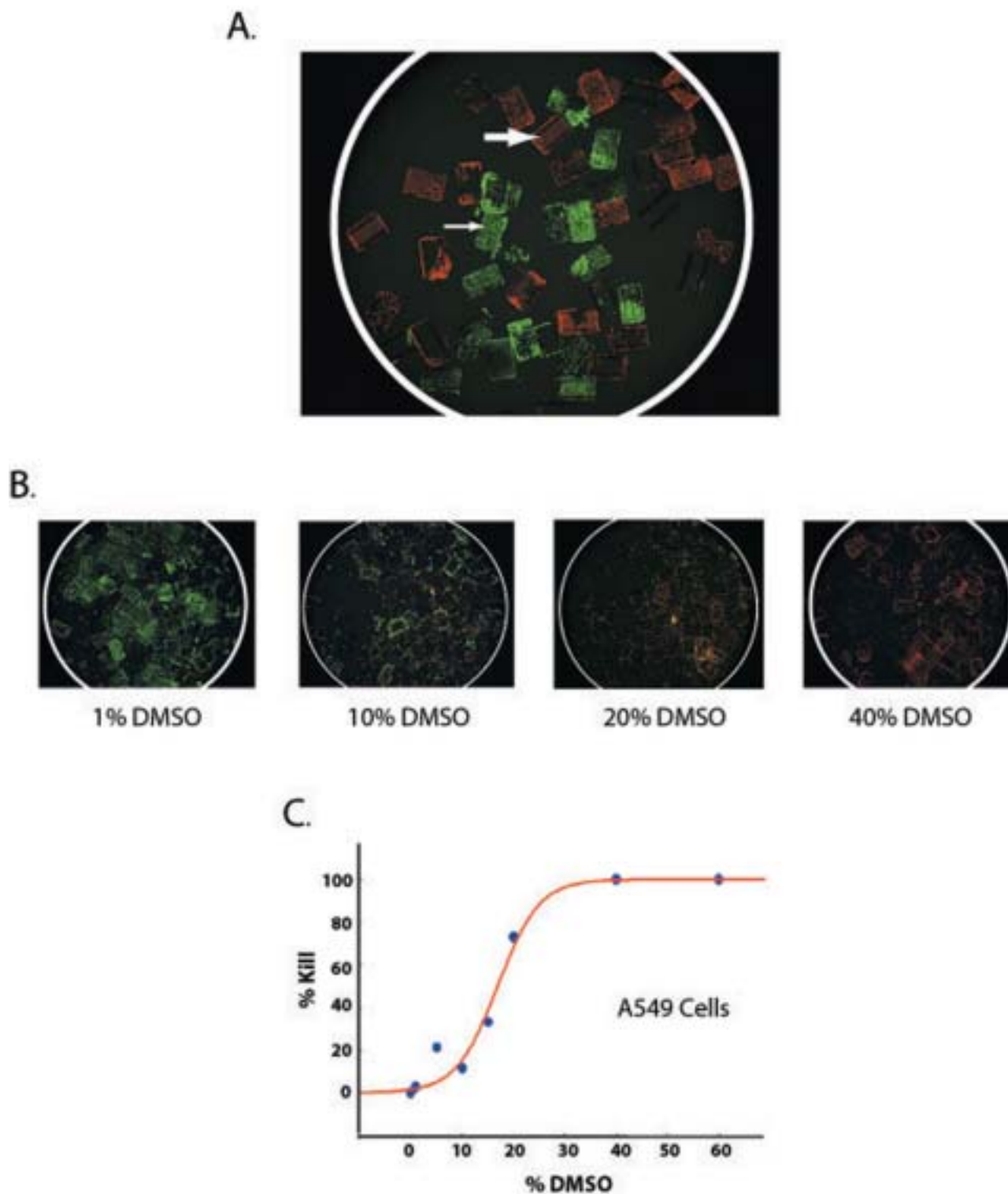


**FIG. 5.** Application of encoded carrier technology to the live-dead cytotoxicity assays. (A) An image of positive (dead) and negative (live) control cells on carriers after staining. Those cells with compromised membranes (dead) stain red (large arrow), whereas those with intact membranes (live) stain green (small arrow). (B) Representative fluorescent images from the multiplexed DMSO dose curve. At low concentrations of DMSO, the majority of cells stain green. As the concentration increases, the cellular membranes are increasingly compromised, and the cells stain red. To decode this array, bright-field images were also taken (data not shown). (C) Nine cell lines were multiplexed in a DMSO dose curve using the live-dead assay. This graph shows the quantified data for A549 cells and is representative of curves for the other 8 cell lines (data not shown).

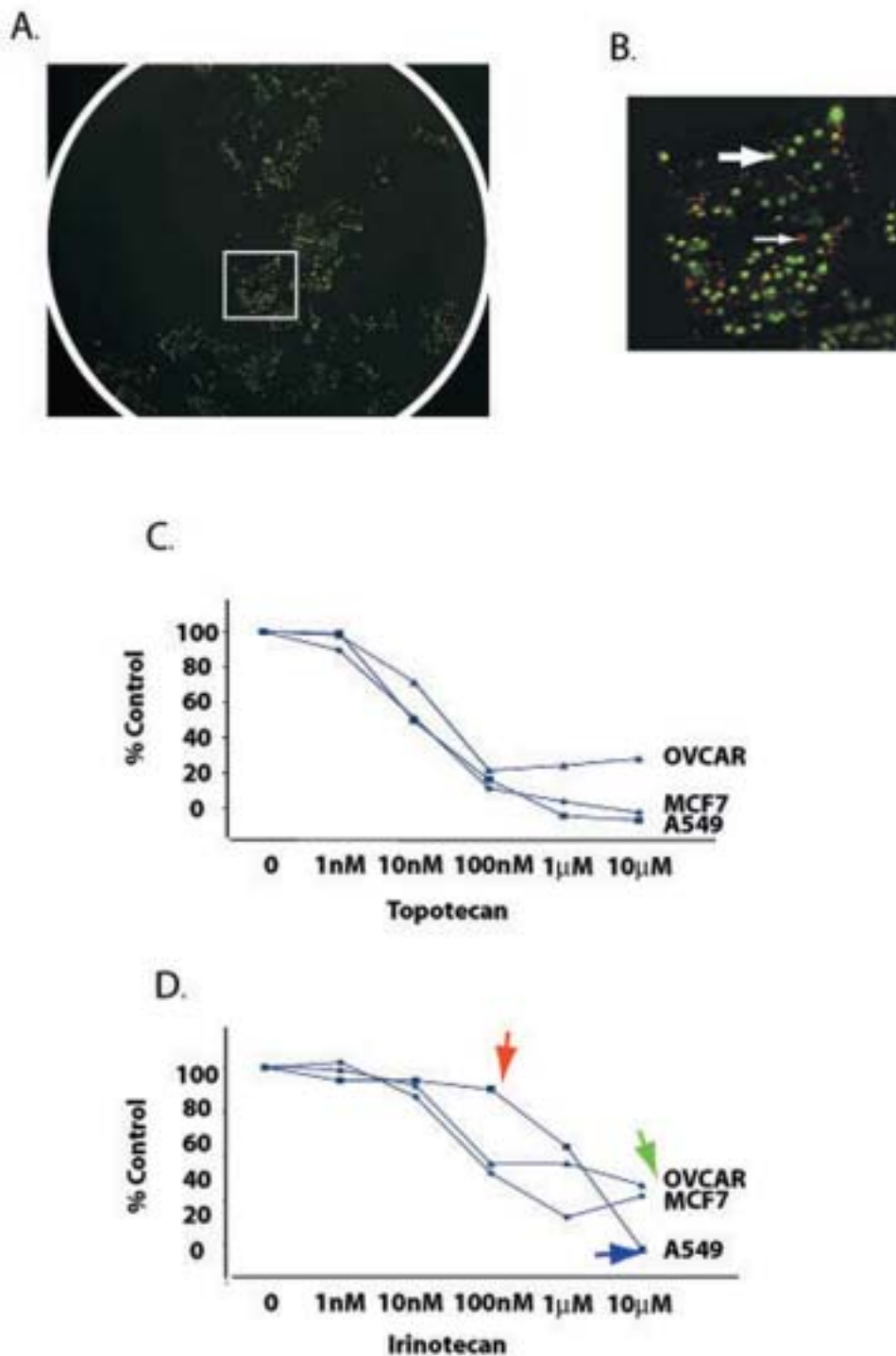


**FIG. 6.** Multiplexed 5-Bromo-deoxyuracil (BrdU) incorporation assay. (A) An image of an entire well showing BrdU incorporation (green spots) in the nuclei of S-phase cells. The red staining is that of the nuclei that were not in S-phase during the BrdU labeling period. The box indicates the area expanded in panel B. (B) Expanded section of the whole well image shown in panel A. The large arrow indicates the nuclei of the cells that incorporated BrdU (green staining). The small arrow indicates the nuclei of a cell that did not incorporate BrdU (red staining). (C-D) Dose curve analysis of 2 proliferation inhibitors, topotecan and irinotecan. This experiment was multiplexed across 3 cell lines: OVCAR3 (triangles), MCF7 (diamonds), and A549 (squares). The data were quantified and normalized, with no drug equaling 100%. Panel C shows that topotecan has very similar effects on each of the 3 cell lines, whereas panel D demonstrates that irinotecan, a very close chemical relative of topotecan, shows differential effects on the 3 cell lines. Notably, A549 cells show a marked resistance to this drug (red arrow).

dispensed into a 96-well microplate format, and stained according to the BrdU incorporation protocol. The merged 7AAD (red, all nuclei) and BrdU (green, BrdU positive nuclei) images from this experiment are shown in Figure 6A. An expanded view of the section of the image within the box is shown in Figure 6B. The nuclei appear as dots that are either red or varying shades of yellow/green. The red nuclei (small arrow) represent those cells that were not in the DNA synthesis (S) phase of the cell cycle during the BrdU labeling period, whereas varying shades of yellow/green (large arrow) correspond to those cells that incorporated differing amounts of BrdU into their DNA. This experiment shows that this encoded particle technology is compatible with a rather complicated assay protocol involving an extended incubation (48 h; see experimental protocol) of the cells on the particles as well as the metabolic labeling of living cells.

Given the utility of this assay in characterizing potential cancer therapeutics, we multiplexed the BrdU incorporation assay across 3 tumor cell lines from different tissue origins: MCF-7 (breast), OVCAR (ovarian), and A549 (lung). Dose curves were then performed with 2 mechanistically related antiproliferatives, topotecan and irinotecan (Fig. 6C,D). As expected, with increasing concentrations of these drugs, there is a concomitant decrease in BrdU incorporation for each of the 3 cell lines. In the case of topotecan, the drug shows nearly identical dose curve profiles for each of the cell lines (Fig. 6C).

Interestingly, despite nearly identical mechanisms, the irinotecan curves are very different from those of topotecan. Although each cell line demonstrates decreased proliferative activity in the presence of increasing drug concentration, the effects differ between cell types. A general difference between the 2 graphs can be seen at 10 nM, where for each cell type, 10 nM topotecan shows a 30% to 40% decrease in BrdU labeling, whereas 10 nM irinotecan had no effect. However, A549 cells show a marked resistance to irinotecan when compared to the other 2 cell lines. At 100 nM irinotecan, there is no effect on A549 BrdU incorporation (red arrow), whereas MCF7 and OVCAR cells are inhibited 50% to 60%. The BrdU incorporation in A549 cells then rapidly drops to zero at 10  $\mu$ M (blue arrow), whereas the others plateau with BrdU incorporation at 30% to 40% of untreated cells (green arrow). The biological mechanisms for these cell type differences are likely very complex. However, by gathering this information from a multiplexed format, one can be certain that each cell type experienced identical incubation conditions, eliminating the possibility that experimental error could have generated these differences. In fact, there have been many reports of interesting metabolic and pharmacological cell-type-specific differences between these 2 compounds.<sup>22-24</sup> This demonstrates that a rather complicated cell-based BrdU incorporation assay can be multiplexed using this encoded particle platform. Furthermore, in doing so, we were able to identify cell-type-specific differences in antiproliferative responses to 2 known antiproliferatives.

Many new technologies seek to increase both information density and quality gathered from experiments. Array technologies, both positional and nonpositional,<sup>6,7,25,26</sup> have provided an efficient way to do this. Multiplexing experiments within a single well increases information density by simultaneously obtaining data on multiple analytes within a single well.<sup>11,17,26</sup> The increase in data quality and robustness is derived from the ability to include internal controls and to correlate data obtained from identical reaction conditions.<sup>26</sup> The nonpositional array technology presented here provides a platform that enables this type of analysis to be done with a diverse set of cellular assays.

We demonstrate that by multiplexing imaging-based cellular assays, both selectivity and activity information can be obtained from a single well. This not only decreases reagent usage but also ensures that each cell type experiences identical conditions (i.e., pipetting errors, evaporation, etc.). In addition, we have also demonstrated the ability to include internal controls for reagent addition, image acquisition, analysis, and mechanism within the same well (Fig. 4). Taken together, this approach simultaneously generates data regarding potency, selectivity, and, with the inclusion of the proper controls, mechanism (Fig. 4C).

Understanding cell-type-specific differences plays an important role in dissecting many mechanisms of disease. For example, the comparison of transformed tumor tissue with normal tissue has led to the identification of many oncogenes and tumor-specific markers.<sup>27,28</sup> Therefore, with increasing knowledge of cancer etiology, it has become possible to screen for potential therapeutics that demonstrate unique cell-type selectivities. One such screen has already been successfully accomplished, looking for compounds that selectively inhibit the growth of mutated K-Ras-transformed cells.<sup>17</sup> In this screen, 2 isogenic (differing only in their K-Ras allele status) cell lines were separately labeled using spectrally unique fluorescent proteins, cocultured, and used to screen nearly 30,000 compounds for antiproliferative activity. This simple multiplexed approach yielded a novel cytidine analog that demonstrated *in vitro* selectivity and inhibited the growth of a mutant K-Ras-containing tumor in a xenograph model. Using this encoded particle technology, this screening methodology can be expanded to include other isogenic cell lines and transformation factors. We expect the results of such a screen to identify compounds whose antiproliferative activity can differentiate between normal and tumor tissues as well as between different mechanisms of transformation. This unique approach to experimental design will provide insight into novel strategies for identifying selective antitumor agents.

This novel platform is compatible with a diverse range of cellular assays. These assays range in nature from being biochemical (i.e., cytokine capture; data not shown) to live cell assays requiring a 48-h incubation with compound (Fig. 6). By enabling the performance and analysis of such diverse assays, the use of this technol-

ogy will provide a unique insight into the profiling of compounds for potency, selectivity, and mechanistic activities.

## EXPERIMENTAL PROTOCOL

### *Encoded carriers*

The encoded carriers were inspected to ensure proper size and coloration. The ECs can be made from multiple materials, including but not limited to acrylics, other polymers, and glass. Prior to their use, the particles are profusely washed with distilled water and coated overnight with 3% poly-L-lysine (Sigma, St. Louis, MO). The poly-L-lysine was then removed and the ECs washed at least 3 times with a large volume of phosphate-buffered saline (PBS).

### *Imaging*

Images acquired from 96-well microplates were taken using an automated microscopy system developed at Vitra Bioscience (Mountain View, CA). This system is equipped with bright field as well as standard epifluorescent illumination optics. The images are captured with a monochromatic cooled 12-bit 1360 × 1036 pixel CCD camera (Qimaging, British Columbia, Canada). This automated system uses inverted optics and is designed to acquire images from microplates. The colorimetric  $\beta$ -galactosidase assay was performed in a standard flat-bottom plate (Corning, Akton, MA). The fluorescent experiments were performed in a clear-bottom imaging plate with black walls (Packard Biosciences, Boston, MA).

Both bright-field and fluorescent images were acquired using a Nikon 2X PlanApo objective lens, numeric appearance (NA) = 0.1. Because the camera is monochromatic, the bright-field images are acquired using red, green, and blue filter on the illuminator. These images are then combined within the image acquisition software to generate the color images. The fluorescent images were acquired using the Chroma Technology Corp. (Rockingham, VT) 82000 filter set. Total imaging time for a 96-well plate (3 bright-field images and 2 fluorescent images) was approximately 35 min.

### *Image analysis and quantification*

All image analysis was performed with custom software written in Matlab (Natick, MA). The decoding of the particles is performed by an algorithm that searches the field of view for encoded carriers and identifies the code associated with them. Analysis of the calcium-flux data (Fig. 3) quantified the fluorescent intensity associated with each encoded carrier. Values determined from images taken after ligand addition ( $F_t$ ) were divided by those taken from before ligand addition images ( $F_0$ ). This ratio represents a fold increase in fluorescence and normalizes for differential loading of the calcium-sensitive dye between different cell types. The quantification of the colorimetric  $\beta$ -gal assay is a ratio of stained to

unstained cells. This measure normalized the amount of staining present to the total number of cells in the clear section of the carriers. The live-dead quantification algorithm returns a measurement of the ratio of red-stained cells to all cells (% dead). The BrdU incorporation assay quantification algorithm specifically quantifies the nuclear-specific signal. The nuclear counterstain is used to identify a nuclear measurement mask. The BrdU-specific stain within that nuclear mask is then quantified based on area as well as intensity. The BrdU data are then normalized to a percentage of the signal obtained from a no-drug control.

### *Tissue culture, EC mixing, EC dispensing*

All media and additives were purchased from Invitrogen Life Sciences (Carlsbad, CA). All cells were grown in Dulbecco's modified Eagle's medium (DMEM) supplemented with 10% fetal calf serum and an antibiotic/antimycotic. The cells were grown in a 37 °C incubator buffered with 5% CO<sub>2</sub>. HEK-293, CHO, HeLa, CV1, COS7, A549, 3T3, HCT116, OVCAR3, and MCF7 cells were purchased from ATCC. CHO-hB2 cells were purchased from Euroscreen (Brussels, Belgium).

For experiments in which cells were plated onto encoded carriers, the carriers were first distributed as a monolayer in 6-well plates. The cells were then trypsinized and plated at a density of 3 to 6 × 10<sup>5</sup> cells per well. After cell attachment, the carriers and associated cells were transferred to a 15-mL conical tube and mixed via inversion. They were then dispensed into microplates either manually with a P200 pipette fitted with a wide bore tip or in an automated fashion using a Cavo 9250 liquid-handling station (Cavo Scientific Instruments, San Jose, CA) fitted with custom tips. The cells were then allowed to recover from 3 h to overnight in a tissue culture incubator.

### *Plasmids and hormones*

The CMV- $\beta$ -gal plasmid and the Ecd expression vectors were purchased from Invitrogen (Carlsbad, CA). The CRE- $\beta$ -gal and the MC3 expression vectors were gifts from Dr. Roger Cone (OHSU). The VIP1, VIP2, and PAC1 expression vectors were gifts from Dr. Joe Pisegna (UCLA). The DH receptor expression vector was a gift from Dr. Jeff Reagan (Tularik).

The diuretic hormone was a gift from Dr. Jeff Reagan (Tularik). Carbachol and kallidin were purchased from Sigma. VIP and MSH were purchased from Phoenix Pharmaceuticals (Belmont, CA). Ponasterone A was purchased from Invitrogen (Carlsbad, CA). All other ligands were purchased from Peninsula Laboratories (San Carlos, CA).

### *Calcium flux*

Cells were loaded with 5  $\mu$ M of the calcium-sensitive dye Fluo-4, AM (Molecular Probes, Eugene, OR) for 30 min at 37 °C in a loading buffer (Krebs-HEPES buffer; 118 mM NaCl, 4.7 mM

KCl, 1.2 mM MgSO<sub>4</sub>, 1.2 mM KH<sub>2</sub>PO<sub>4</sub>, 4.2 mM NaHCO<sub>3</sub>, 11.7 mM D-Glucose, 1.3 mM CaCl<sub>2</sub>, 10 mM HEPES [pH 7.4], 0.5% bovine serum albumin [BSA]). Thereafter, cells were washed twice with loading buffer and incubated with fresh loading buffer for 30 min at 37 °C. Prior to ligand addition, an image of the well was acquired. Then, 1 μM kallidin and/or 100 μM carbachol mixture was added to the well, and images were acquired every 2 sec for up to 1 min.

#### β-gal reporter assay

Using Lipofectamine 2000 (Invitrogen, Carlsbad, CA), 293 cells were transiently transfected in 6-cm dishes at 80% to 90% confluency. After 6 h, the cells were washed with fresh media, trypsinized, and split into a well containing a monolayer of encoded carriers. The cells were then allowed to attach and grow overnight in a 37 °C, 5% CO<sub>2</sub> incubator. After mixing and dispensing, the media were removed, and fresh, prewarmed 37 °C media containing the appropriate ligand were added. The cells were then incubated in the tissue culture incubator for 6 h. The cells were then washed once with PBS and fixed with 0.35% glutaraldehyde (Sigma, St. Louis, MO) in 25 mM HEPES (pH 7.2) for 10 min. The cells were then washed 3 times with PBS and stained with X-gal using a staining kit purchased from Invitrogen (Carlsbad, CA). The staining was allowed to develop overnight at 37 °C. The staining solution was then removed and replaced with PBS prior to imaging in bright field.

#### Live-dead assay

For the feasibility experiment, cells were grown on ECs with unique codes and then either left untreated or treated with cold 100% methanol for 10 min before staining. For the dose curve experiment, the media were replaced with media containing increasing concentrations of DMSO and incubated for 24 h in the tissue culture incubator. Live-dead staining occurred via the protocol supplied by Molecular Probes (Eugene, OR). Briefly, the media was removed, and 75 μL of staining solution was added. The cells were then incubated in the tissue culture incubator for 30 min, protected from light. The plate was then imaged in FITC and CY3 channels.

#### BrdU incorporation assay

Irinotecan and topotecan were added separately to wells with log fold dilutions. The plates were then incubated for 48 h at 37 °C, 5% CO<sub>2</sub>. The drugs were removed, and 10 μM BrdU labeling solution (purchased as a kit from Roche Molecular Biochemicals, Indianapolis, IN) was added to cells for 4 h. Labeling medium was then removed, and cells were fixed with the FixDenat solution provided in the kit for 30 min. Then, cells were washed twice with PBST (PBS containing 0.1% Tween-20) and incubated with 1:40 dilution of Alexa Fluor-488-conjugated anti-BrdU antibody (Molecular Probes, Eugene, OR) for 2 h at room temperature. Cells were

washed 3 times with PBST and 3 times with PBS, and then they were incubated with 4 μg/mL 7-AAD (Molecular Probes, Eugene, OR) for 1 h at room temperature. The plates were then imaged in bright-field, FITC, and CY3 channels.

#### ACKNOWLEDGMENTS

We thank Roger Cone, Joe Pisegna, and Jeff Reagan for the generous reagent gifts and discussions. In addition, we would like to thank Peter Lamb and Peiwen Yu for discussions about the BrdU incorporation assay results.

#### REFERENCES

1. Brown PO, Botstein D: Exploring the new world of the genome with DNA microarrays. *Nat Genet* 1999;21:33-37.
2. Eickhoff H, Konthur Z, Lueking A, Lehrach H, Walter G, Nordhoff E, et al: Protein array technology: the tool to bridge genomics and proteomics. *Adv Biochem Eng Biotechnol* 2002;77:103-112.
3. Anthony RM, Brown TJ, French GL: DNA array technology and diagnostic microbiology. *Expert Rev Mol Diagn* 2001;1:30-38.
4. Bussow K, Konthur Z, Lueking A, Lehrach H, Walter G: Protein array technology: potential use in medical diagnostics. *Am J Pharmacogenomics* 2001;1:37-43.
5. Groves JT: Membrane array technology for drug discovery. *Curr Opin Drug Discov Devel* 2002;5:606-612.
6. Nolan JP, Mandy FF: Suspension array technology: new tools for gene and protein analysis. *Cell Mol Biol* 2001;47:1241-1256.
7. Zhou H, Roy S, Schulman H, Natan MJ: Solution and chip arrays in protein profiling. *Trends Biotechnol* 2001;19:S34-S39.
8. Beske OAG: High-throughput cell analysis using multiplexed array technologies. *Drug Discov Today* 2002;7:S131-S135.
9. Nicewarner-Pena SR, Freeman RG, Reiss BD, He L, Pena DJ, Walton ID, et al: Submicrometer metallic barcodes. *Science* 2001;294:137-141.
10. Chan WC, Maxwell DJ, Gao X, Bailey RE, Han M, Nie S, et al: Luminescent quantum dots for multiplexed biological detection and imaging. *Curr Opin Biotechnol* 2002;13:40-46.
11. Iannone MA, Consler TG, Pearce KH, Stimmel JB, Parks DJ, Gray JG, et al: Multiplexed molecular interactions of nuclear receptors using fluorescent microspheres. *Cytometry* 2001;44:326-337.
12. Ziauddin J, Sabatini DM: Microarrays of cells expressing defined cDNAs. *Nature* 2001;411:107-110.
13. Schanstra JP, Bataille E, Marin Castano ME, Barascud Y, Hirtz C, Pesquero JB, et al: The B1-agonist [des-Arg10]-kallidin activates transcription factor NF-kappaB and induces homologous upregulation of the bradykinin B1-receptor in cultured human lung fibroblasts. *J Clin Invest* 1998;101:2080-2091.
14. Yamamoto KK, Gonzalez GA, Biggs WH III, Montminy MR: Phosphorylation-induced binding and transcriptional efficacy of nuclear factor CREB. *Nature* 1988;334:494-498.
15. Gonzalez GA, Montminy MR: Cyclic AMP stimulates somatostatin gene transcription by phosphorylation of CREB at serine 133. *Cell* 1989;59:675-680.
16. Chen W, Shields TS, Stork PJ, Cone RD: A colorimetric assay for measuring activation of Gs- and Gq-coupled signaling pathways. *Anal Biochem* 1995;226:349-354.

## Simultaneous Interrogation of Multiple Cell Types

---

17. Torrance CJ, Agrawal V, Vogelstein B, Kinzler KW: Use of isogenic human cancer cells for high-throughput screening and drug discovery. *Nat Biotechnol* 2001;19:940-945.
18. Weinstein JN, Buolamwini JK: Molecular targets in cancer drug discovery: cell-based profiling. *Curr Pharm Des* 2000;6:473-483.
19. Papadopoulos NG, Dedoussis GV, Spanakos G, Gritzapis AD, Baxevanis CN, Papamichail M, et al: An improved fluorescence assay for the determination of lymphocyte-mediated cytotoxicity using flow cytometry. *J Immunol Methods* 1994;177:101-111.
20. Papadopoulos NG, Dedoussis GV, Spanakos G, Gritzapis AD, Baxevanis CN, Papamichail M, et al: Effects of tamoxifen on potential doubling time of human breast cancer cell line determined by image cytometry of double fluorescent BrdU and DNA labeling. *Anticancer Res* 1994;14:2025-2032.
21. Khaing ZZ, Blum M: Detection of cell proliferation and cell fate in adult CNS using BrdU double-label immunohistochemistry. *Methods Mol Med* 2003;79:499-505.
22. Mathijssen RH, Loos WJ, Verweij J, Sparreboom A: Pharmacology of topoisomerase I inhibitors irinotecan (CPT-11) and topotecan. *Curr Cancer Drug Targets* 2002;2:103-123.
23. Rostagno P, Moll JL, Birtwisle-Peyrottes I, Ettore F, Lagrange JL, Gioanni J, Caldani C, et al: Differential activity of topotecan, irinotecan and SN-38 in fresh human tumour cells but not in cell lines. *Eur J Cancer* 2000;36:2120-2127.
24. Jones SF, Burris HA III: Topoisomerase I inhibitors: topotecan and irinotecan. *Cancer Pract* 1996;4:51-53.
25. Armstrong B, Stewart M, Mazumder A: Suspension arrays for high throughput, multiplexed single nucleotide polymorphism genotyping. *Cytometry* 2000;40:102-108.
26. Martins TB: Development of internal controls for the Luminex instrument as part of a multiplex seven-analyte viral respiratory antibody profile. *Clin Diagn Lab Immunol* 2002;9:41-45.
27. Nam NH, Parang K: Current targets for anticancer drug discovery. *Curr Drug Targets* 2003;4:159-179.
28. Srinivas PR, Verma M, Zhao Y, Srivastava S: Proteomics for cancer biomarker discovery. *Clin Chem* 2002;48:1160-1169.

Address reprint requests to:  
Oren Beske  
Vitra Bioscience, Inc.  
2450 Bayshore Parkway  
Mountain View, CA 94043

E-mail: [obeske@vitrabio.com](mailto:obeske@vitrabio.com)